Coupled simulations and comparison with multi-lidar measurements of the wind flow over a double-ridge

Veiga Rodrigues, C.; Palma, J.M.L.M.; Vasiljevic, Nikola; Courtney, Michael; Mann, Jakob

Published in:
Journal of Physics: Conference Series (Online)

Link to article, DOI:
10.1088/1742-6596/753/3/032025

Publication date:
2016

Document Version
Publisher's PDF, also known as Version of record

Coupled simulations and comparison with multi-lidar measurements of the wind flow over a double-ridge

2016 J. Phys.: Conf. Ser. 753 032025

(http://iopscience.iop.org/1742-6596/753/3/032025)

Coupled simulations and comparison with multi-lidar measurements of the wind flow over a double-ridge

C Veiga Rodrigues[1], JMLM Palma[1], N Vasiljević[2], M Courtney[2], and J Mann[2]

[1] Departamento de Engenharia Mecânica, Faculdade de Engenharia da Universidade do Porto, Portugal
[2] DTU Wind Energy, Risø campus, Roskilde, Denmark

E-mail: cvr@fe.up.pt

Abstract. The wind flow over a double-ridge site has been numerically simulated with a nested model-chain coupling, down to horizontal resolutions of 40 m. The results were compared with field measurements attained using a triple-lidar instrument, the long-range WindScanner system, which allowed measurements up to 500 m height and the mapping of the wind speed onto a two-dimensional transect crossing the valley. The site, known as Serra do Perdigão, is located in central Portugal and consists of two parallel ridges 1.4 km apart with height differences of 200 m in between, being characterized by rough terrain and forested areas. The analysis was restricted to June 10$^{\text{th}}$ 2015, for which measurements and simulations both predicted gravity wave activity, the later showing formation of rotors in the lee of both ridges and some events of wave breaking above the ridge top.

1. Introduction

Field measurements of the atmospheric flow usually consist of point mast-mounted probes, commonly a set of cup anemometers and wind vanes. Although such measurements are paramount to assess the performance of numerical flow solvers, mast instrumentation is usually placed at locations suitable for wind resource assessment and without the purpose of characterizing the flow field. In complex terrain, ridge tops and mountain summits are natural choices, however in the perspective of modelers it is in the valleys and mountain slopes that most interesting flow phenomena happens.

State of the art techniques in remote-sensing instrumentation, for instance [1, 2], allow for field measurements which are not limited to point measurements, but may produce maps of the flow field along two-dimensional surfaces or three-dimensional volumes. Although with limitations regarding the characterization of turbulence statistics, mainly due to the compromise between mapping a large surface or sampling at a point-like location, these novel techniques offer insight into zones where the flow is seldom characterized. Such instruments allow for higher detail in field measurements focusing wind-energy applications, closer to that found in scientific field experiments (e.g. [3]).

In the present study, numerical flow simulations are compared with field measurements results for Perdigão, a double-ridge site characterized by rough terrain and forested areas. The purpose was to infer details of the flow field over a wide area through numerical simulation, as an aid in the design of the future Perdigão-2017 experiment [4, 5], while using the measurements to qualitatively assess the simulation results. The measurements were performed using a triple-lidar instrument, namely the long-range WindScanner (LRWS) system [1], which allowed the

measurement of the flow field over a transect surface normal to the ridges, thus capturing the valley flow over the course of a whole day, June 10th 2015. Numerical simulations covering that period were performed with a model-chain approach consisting of the Weather Research and Forecasting (WRF) [6] and the VENTOS®/M [7] unsteady Reynolds-averaged Navier-Stokes (URANS) atmospheric flow solver, resulting in a three-dimensional time-dependent dataset of the flow field.

The remainder of this paper consists of the following sections: in Section 2 are described the experimental and numerical methods, the results are shown and analysed in Section 3 and the conclusions are presented in Section 4.

2. Methodology

2.1. Description of the site and field experiment

During the months of May and June 2015 a large field campaign –*Perdigão 2015*– took place at the site of Serra do Perdigão, located in central Portugal [8]. Figure 1 shows the site topography which consists of two 4 km long parallel ridges, about 1.4 km away from each other. The south-west (SW) ridge has a 2 MW wind turbine.

The LRWS system was employed at the site, thus three scanning lidars, to acquire mean wind field measurements over a large area. The lidar *Whittle* was located on the SW ridge near the wind turbine, whereas the other two lidars, *Koshava* and *Sterenn* were placed on the opposite ridge (Fig. 1). The three lidars were configured to three scanning strategies denoted as the *virtual mast scan*, *ridge scan* and *diamond scan*. For the scope of the present paper only the virtual mast scan and the ridge scan are described. For details on the diamond scan, please refer to [9]. The virtual mast, ridge and diamond scans were run in a batch mode, thus one scan after another.

The virtual mast scan consisted of three synchronized range-height indication (RHI) scans, during which Whittle, Sterenn and Koshava intersected their laser beams at the valley bottom

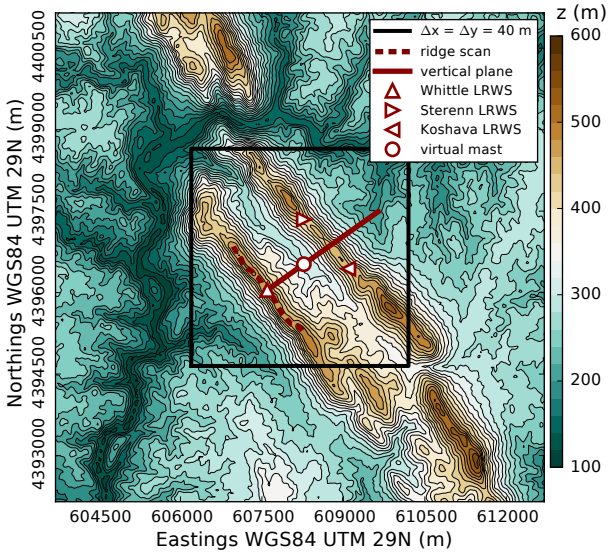

Figure 1: Map of Serra do Perdigão. The red line depicts the vertical transect used by the LRWS system. The map limits coincide with the VENTOS®/M domain. The horizontal grid resolution inside the black square was 40 m.

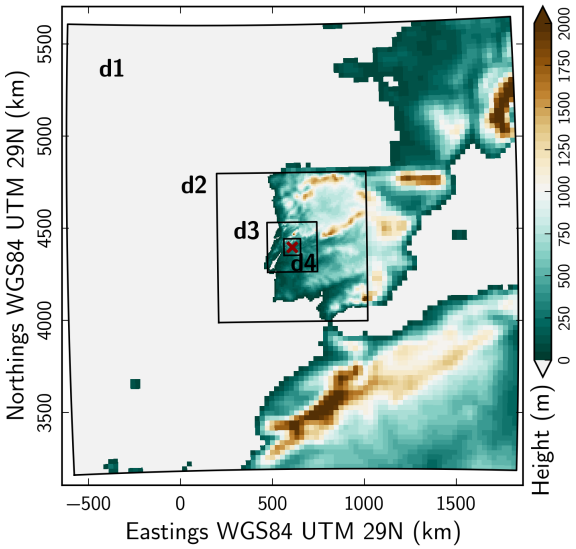

Figure 2: Setup of the WRF domains used in the simulations, consisting of four nestings with horizontal grid resolutions of 27, 9, 3 and 1 km.

and moved the beam intersection along a 500 m tall virtual mast (dashed line in Figs. 4-6). The angle measured in a horizontal plane between any two laser beams was 60°. One iteration of the transect scan took 25 s where a set of three independent radial velocities was acquired every 10 m (50 measurement points). The probe length of each individual lidar was set to 30 m. The position of the range gates along the virtual mast were optimized to provide grounds for the intersection of the three laser beams. As three independent radial velocities were measured and since the angle between any two laser beams was 60°, there was a favorable environment to accurately convert radial velocities into horizontal wind speed and wind direction. The accuracy of resolving horizontal wind speed and wind direction in complex terrain by means of employing the LRWS system is discussed in [10].

Due to interference of trees and ground, the first 12 measurement points were screened out from the measurement dataset, therefore the virtual mast was operational from 120 to 500 m above ground level (agl). Besides resolving the horizontal wind speed and wind direction at the virtual mast, Whittle was used to map the radial velocity field in 12050 measurement points over a vertical plane perpendicular to the ridges, a vertical transect entailing the virtual mast.

For the ridge scan, Koshava and Sterenn were employed to intersect the laser beams and to move the beam intersection 80 m agl along a 2 km long path over the SW ridge, resolving the horizontal wind speed and wind direction in 100 measurement points. For the scope of this paper a single measurement point close to the Whittle location has been selected and analyzed (Fig. 3 top).

2.2. Numerical simulations

The flow simulations were performed with a model chain consisting of the WRF model [6] and VENTOS®/M [7] computer codes. The WRF model is a numerical weather prediction code mostly used for simulation of the atmospheric flow at a regional level. The VENTOS®/M model is an URANS flow solver operating with WRF results through a one-way dynamical coupling.

The WRF model simulations used four nests with horizontal resolutions ranging from 27 to 1 km following a 1/3 ratio rule (Fig. 2). All domains used a $90\times90\times60$ grid and the time step was set to 144, 72, 24 and 3 s respectively. These simulations were driven using ERA-Interim reanalysis datasets [11]. Parameterization of the planetary boundary layer was achieved with the Mellor–Yamada Nakanishi Niino (MYNN) level 2.5 model and surface fluxes were modelled with the unified NOAH land-surface scheme.

These results were further downscaled with the VENTOS®/M model to 40 m resolution at the site of interest through a variable-resolution computational grid (Fig. 1) expanding to 990 m at the domain boundaries. The horizontal grid was composed by 144×144 control volumes and the vertical domain consisted of 10 km columns of 66 control volumes, expanding from 4 m near the surface to 830 m at the domain top, where a 3.5 km Rayleigh damping layer was set. The simulation time step was 1.5 s and the boundary conditions were updated every 5 minutes, having been sampled from the 1 km WRF model results.

The orography for the WRF 1 km and VENTOS®/M surface grids was generated using the Shuttle Radar Topography Mission (SRTM) datasets, resampled according to grid resolution. Land-use categories for all domains were based on the CORINE Land Cover 2006 inventory (by conversion to U.S. Geological Survey classes [12]) resulting in aerodynamic roughnesses at the site of 3, 4.2 and 20 cm for the 25^{th}, 50^{th} and 75^{th} percentiles, respectively.

3. Results

In this section the simulations results are analyzed and compared with the field measurements. Time series for June 10^{th} 2015 are presented first with the whole period that was covered by the simulations. Further analysis of the results focus the early morning period that was characterized by formation of gravity waves, by resorting to the flow visualization along a vertical transect.

An analysis of the flow three-dimensionality is performed by showing flow streamlines in several horizontal surfaces. In the final section, two gravity wave regimes predicted by the simulations are examined.

3.1. Timeseries

Figure 3 top shows three distinct periods. The first period corresponds to the start of the simulations up to 21:00 LT (local time) of June 9, where the simulation results show large variability, some in agreement with the measurements. A second period happens during the morning of June 10, up to 8:00 LT, where the simulation results are apparently out-of-phase, predicting lower speeds at midnight conversely to the measurements. It is also the period where the wind direction agreement is bad, with errors higher than 90°. The simulations predict winds flowing from S–SW whereas the measurements show E–NE winds. The 9 km WRF model solution performs better than its nestings, both in predicting the magnitude and azimuth. The VENTOS®/M model briefly improves the wind direction prediction, yielding errors of 25°from

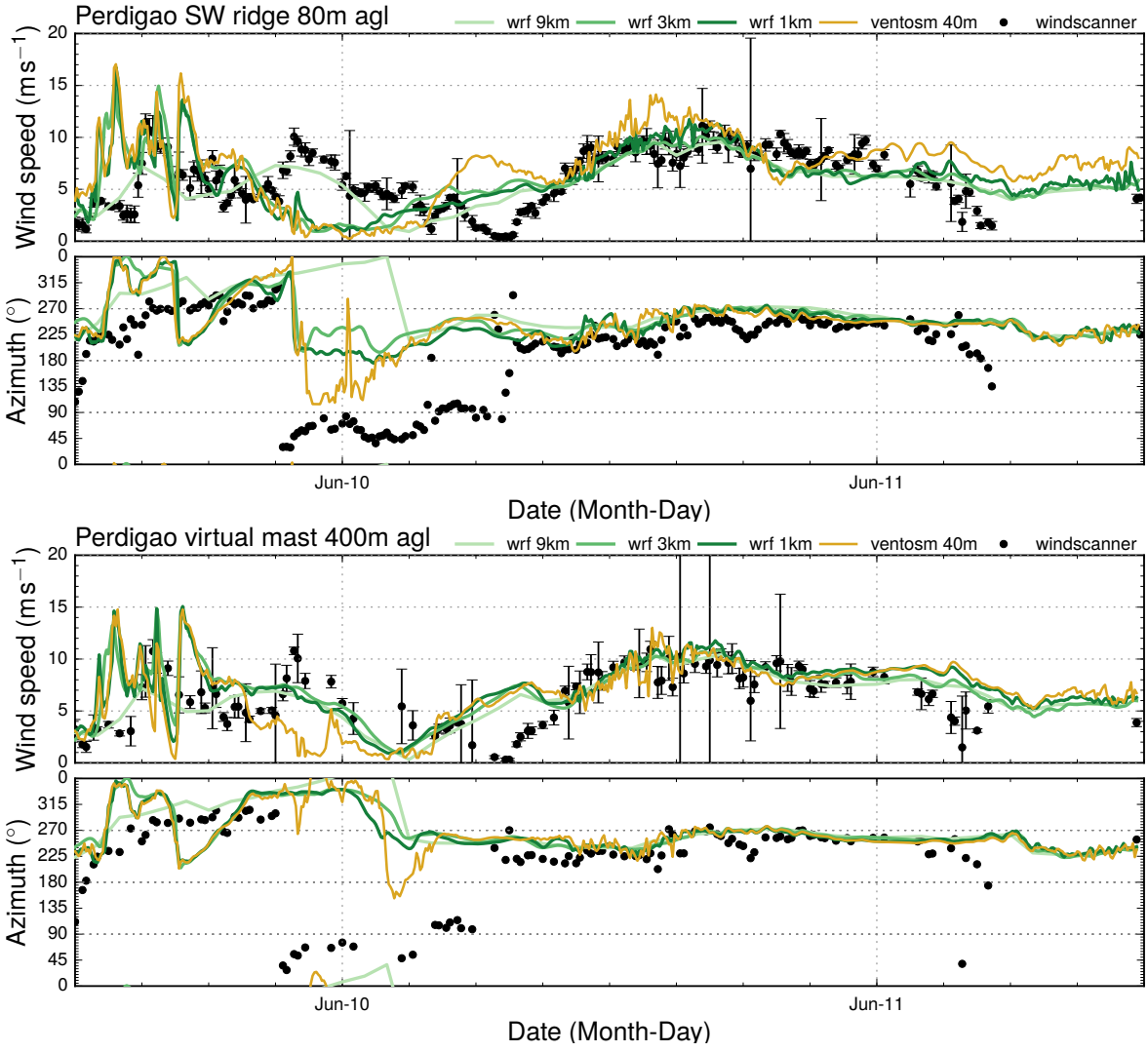

Figure 3: Time series of wind speed and direction for: (top) SW ridge near Whittle LRWS and (bottom) Virtual Mast location in the valley. Error bars denote 95% confidence intervals.

22:00 to 1:00 LT. The third period happens throughout the remainder of June 10, with a very good agreement between the simulations results and measurements, both in magnitude and in predicting S–SW winds.

The simulations results for the second period are characterized by wind speeds below $3\,\mathrm{m\,s^{-1}}$. The prediction of low wind speeds by numerical models is associated with high error in the wind direction forecast [7, 13], a trait evident in Fig. 3. Conceptually URANS turbulence models assume high Reynolds number flow. Albeit the Reynolds number at low wind speeds is very large, flow characteristics such as turbulence intensity, shear factor [14] and wind-direction error [7] show an inversely proportional trend with the wind speed, suggesting a dependence on the Reynolds number. Hence, an hypothesis for the wind-direction error is the failure of turbulence models in replicating all characteristics of low wind-speed regimes. However, a clear explanation for this performance breakdown is yet to be found.

Although the virtual mast was located at the valley, its measurements (Fig. 3 bottom) are very similar to the SW ridge data (Fig. 3 top).

3.2. Vertical transects

Figure 4 shows the flow field in a transect plane cross-cutting the ridges, as predicted by the simulations (Fig. 4top) and acquired by the Whittle LRWS system mounted at the first ridge (Fig. 4bottom). The transect plane was the line-of-sight field viewed by Whittle LRWS system, extending down to 2.5 km away along the 55°–235° azimuth, covering the valley and the flow above the second ridge. The velocity measured was the component in the radial direction to the scan (the speed along the line-of-sight vector) thus its value is dependent on the beam angle with the horizontal plane, which varied between -13° and 21°.

The contour map shown in Fig. 4top is representative of wind field at daytime, where the agreement of numerical results with the measurements was good. Both contour maps in Fig. 4 are similar and, apart from slightly higher wind speeds above 1 km height, the simulations were able to reproduce both the wake of the first ridge and flow speed-up at the top of the second ridge.

Figure 5 shows the flow field for early morning hours around 3:30 LT (radial velocity fields like Fig. 4). Although the agreement at nighttime was worse (Fig. 3) this was the period where the measurements have the most interesting meteorological phenomena. Both results in Fig. 5 show undulating patterns in phase with the topography and with half of its wavelength. Flow visualization of the streamlines (Fig. 5top) show horizontally-repeating standing mountain waves with wave breaking in the lee of both ridges at an height of 600 m above mean sea level (amsl). Additionally, the simulation results show rotor formation in the valley and past the second ridge (refer to Section 3.4 for further analysis).

The simulations predict mostly positive radial velocities whilst the measurements show negative values below 700 m amsl. Figure 6 shows the velocity component perpendicular to the transect, quantified according to the simulation results. Two layers are distinguishable, an upper layer with NW winds and a lower layer with a very strong southern component. Hence, the simulations predict that a significant part of flow is crossing the transect plane, except at: (i) the interface between both layers that is located at heights around 700 m amsl and (ii) the zones at the top of both ridges where, due to speed-up effects, the flow is approximately perpendicular to the ridges. As referred to in Section 3.1, the difficulty in predicting the wind direction is greater for low wind speeds [7]. Considering the transect plane direction (55°–235° azimuth) and the predicted wind direction is mostly southern, a error in wind direction higher than 35° is sufficient to have negative radial velocities when projected onto the transect plane. Hence, the negative velocities are consistent with the Fig. 3 time series where 90° differences are seen between 3:00 to 4:00 LT. Despite these significant differences, it is interesting to observe such similar gravity wave patterns between measurements and simulations.

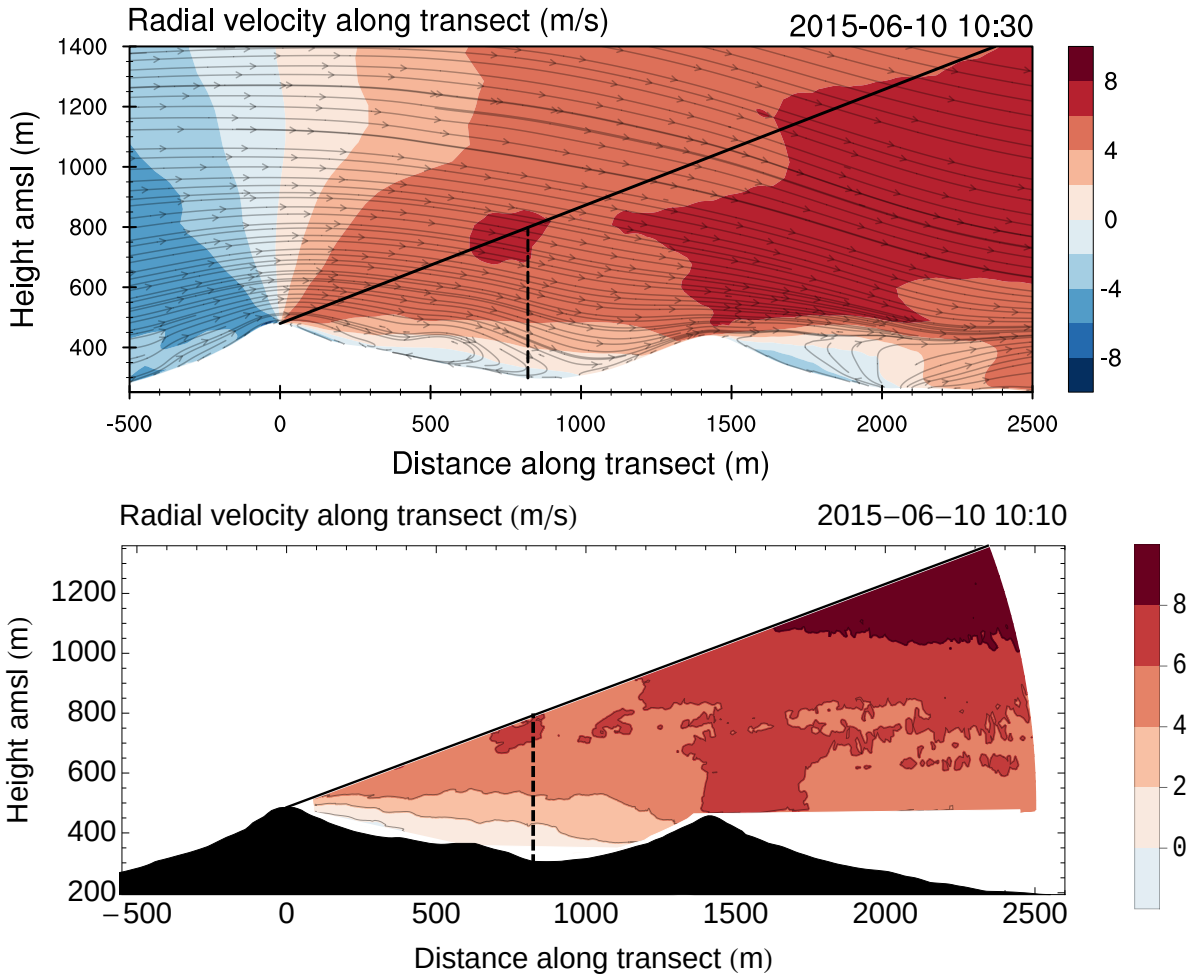

Figure 4: Results for June 10$^{\text{th}}$ 2015, around 10:30 LT for: (top) WRF–VENTOS®/M coupling simulation results and (bottom) Whittle LRWS field measurements. The contour maps show the radial velocity field (negative speed implies flow towards the measurement location). The flow streamlines refer to the velocity vector in the transect plane. The solid line delimits the maximum angle of the transect scan and the dashed line marks the 500 m agl virtual mast.

3.3. Horizontal flow maps

Both the orography of the double-ridge site and the visualization of the vertical transects in Fig. 5 suggest a simple wind flow structure where the wind vectors are mostly aligned with the transect. Despite the difficulties of the simulations in reproducing the actual flow field, the numerical results may be used to infer the three-dimensionality of the wind field.

Figure 7 shows the structure of the flow field for several horizontal surfaces. At 1000 m amsl the wind flows towards east with few differences in the streamline trajectories. Major deflections in the streamlines are visible at 750 m amsl height, where the flow past the second ridge shifts north. At an height of 500 m amsl the wind upstream of the first ridge is also deflected north, implying that the flow lacks energy to overcome the ridge, thus circumventing it. The 400 m amsl horizontal plane allows to visualize the valley winds which is mainly directed towards NW, thus flowing perpendicular to the transect as depicted in Fig. 6, escaping the ridges through the north part. Although the topography is apparently simple, the streamlines in Fig. 7 show a flow whose nature is highly three-dimensional, hindering its analysis when solely visualizing the vertical transects.

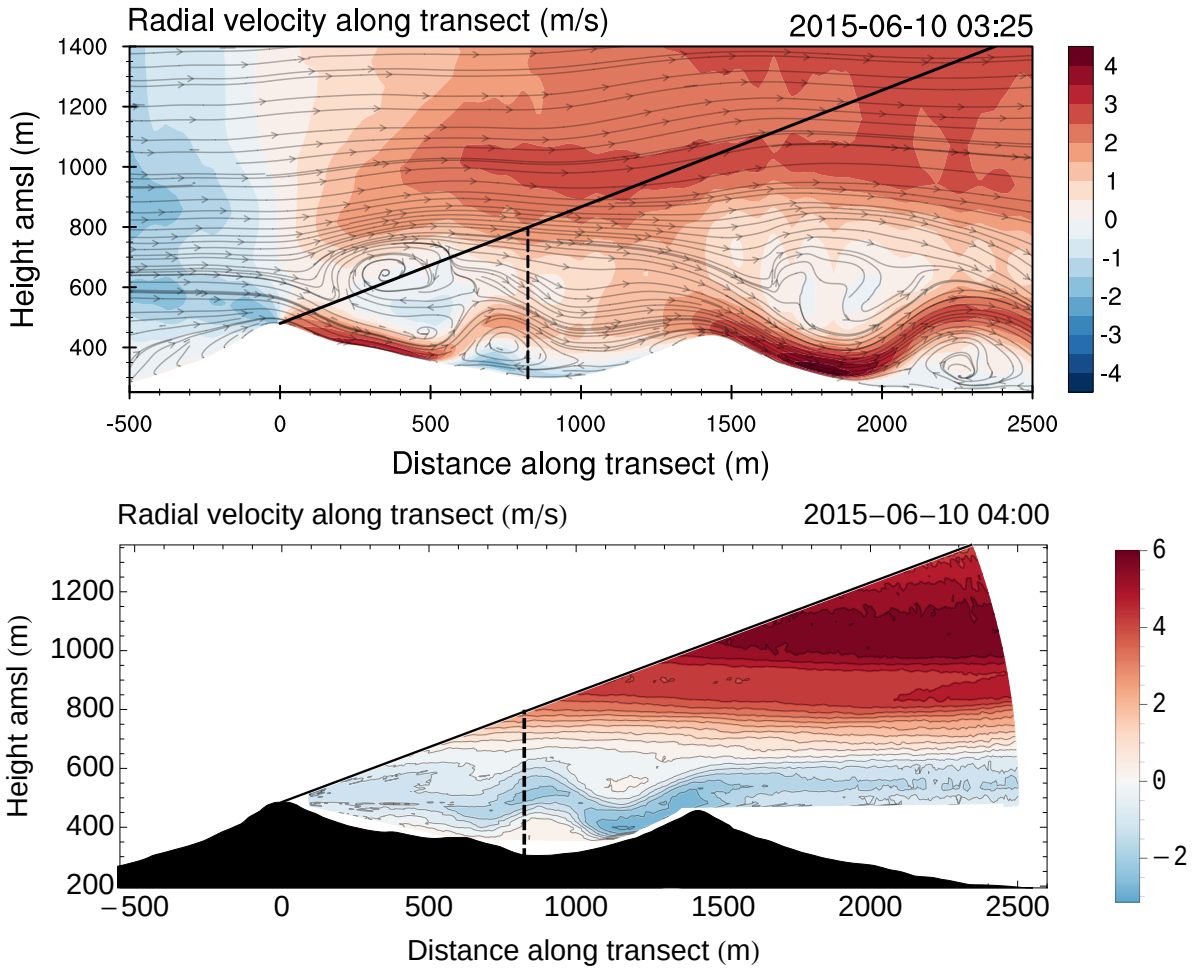

Figure 5: Results for June 10th 2015, between 0300–0400 LT. See Fig. 4 for further details.

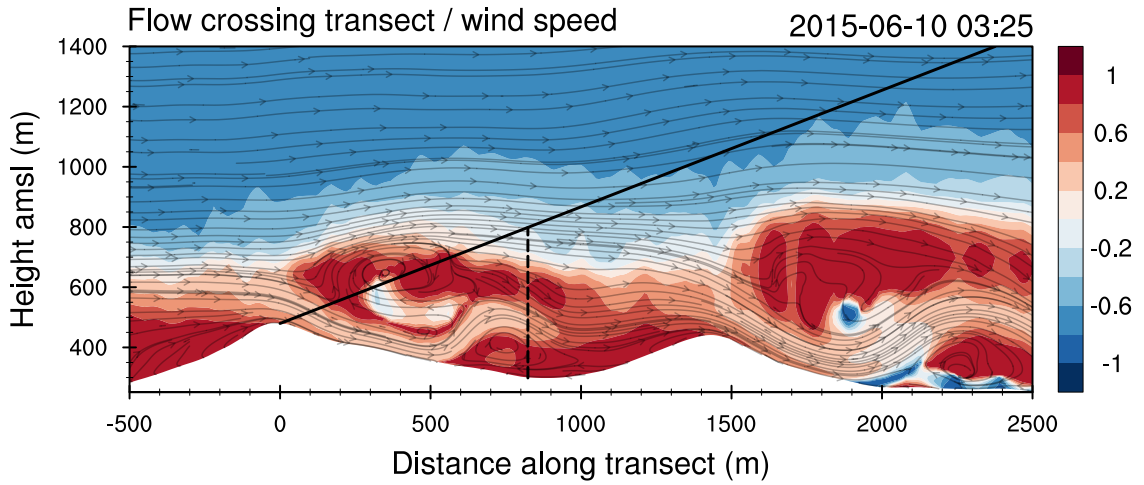

Figure 6: Contour map with fraction of flow crossing the transect in the VENTOS®/M model results for June 10th 2015, 3:25 LT. Positive values indicate velocity vectors pointing towards NW. See Fig. 5 for further details.

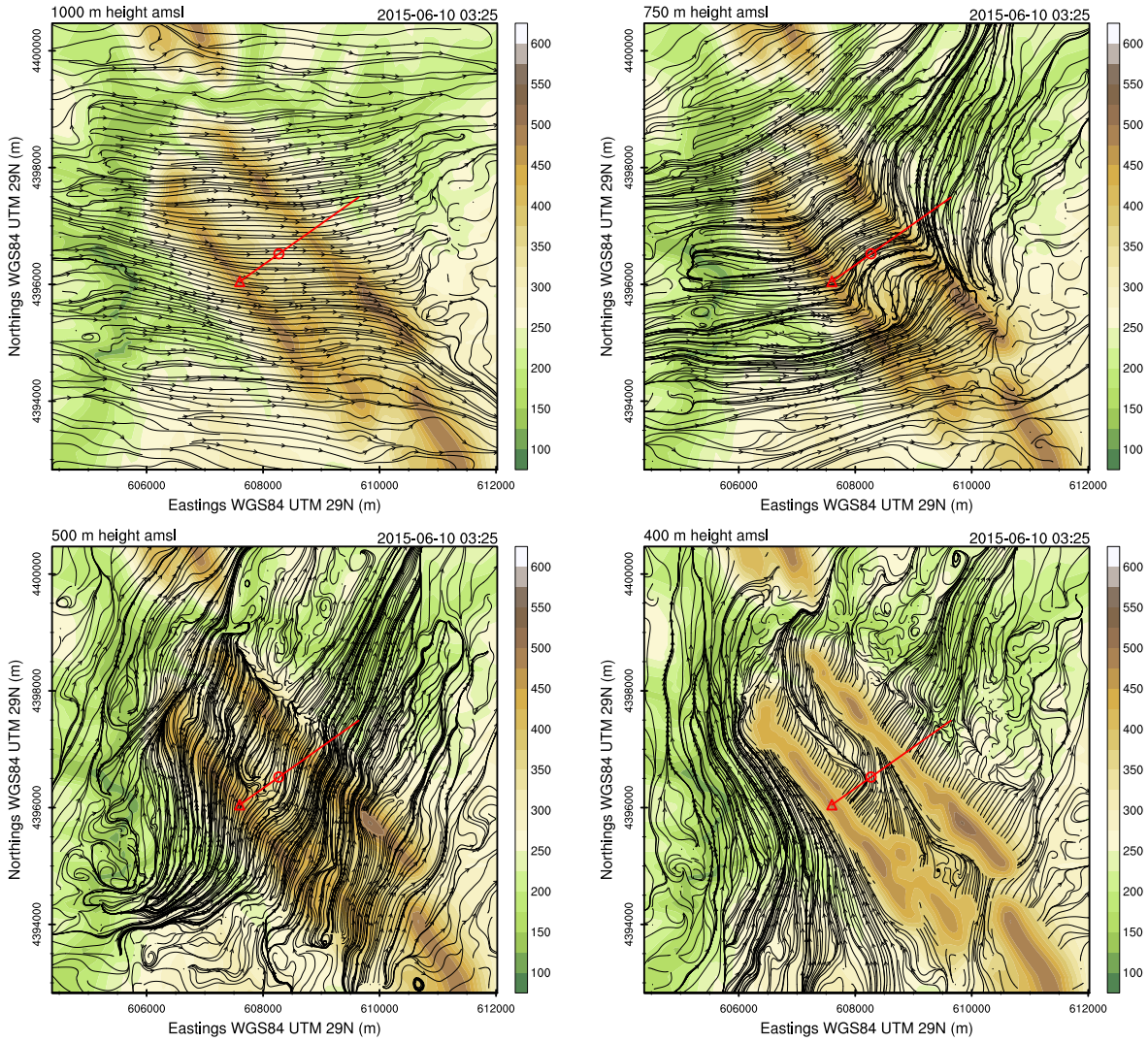

Figure 7: Horizontal surfaces of constant height amsl with flow streamlines from the VENTOS®/M model results of June 10$^{\text{th}}$ 2015, 3:25 LT, for: 1000 m, 750 m, 600 m and 400 m amsl. The contour map refers to the terrain height.

3.4. Gravity waves predicted by the simulations

The numerical simulation results have shown two distinct regimes for the formation of gravity waves, both displayed in Fig. 8.

Following the analysis in Section 3.2, the flow shows lee waves repeating downstream with wave breaking happening after both ridge tops. Figure 8top shows the wave structure down to 4 km past the first ridge. Considering the orography is similar to a double bell shape with 1.4 km wavelength, the wavelength of the gravity waves is approximately half of that value, around 0.75 km. Hence, the waves are in phase with the orography which promotes the formation of two rotors, one at the valley and the other after the second ridge, around 0.7 and 2.3 km relative to the first ridge.

A second regime was observed (Fig. 8bottom) where the wavelength of the waves is approximately that of the orography. Whereas the leeward rotor is displaced to 2.6 km, implying a wavelength of 1.3 km, the valley rotor is suppressed as its existence would be out-of-phase with the waves.

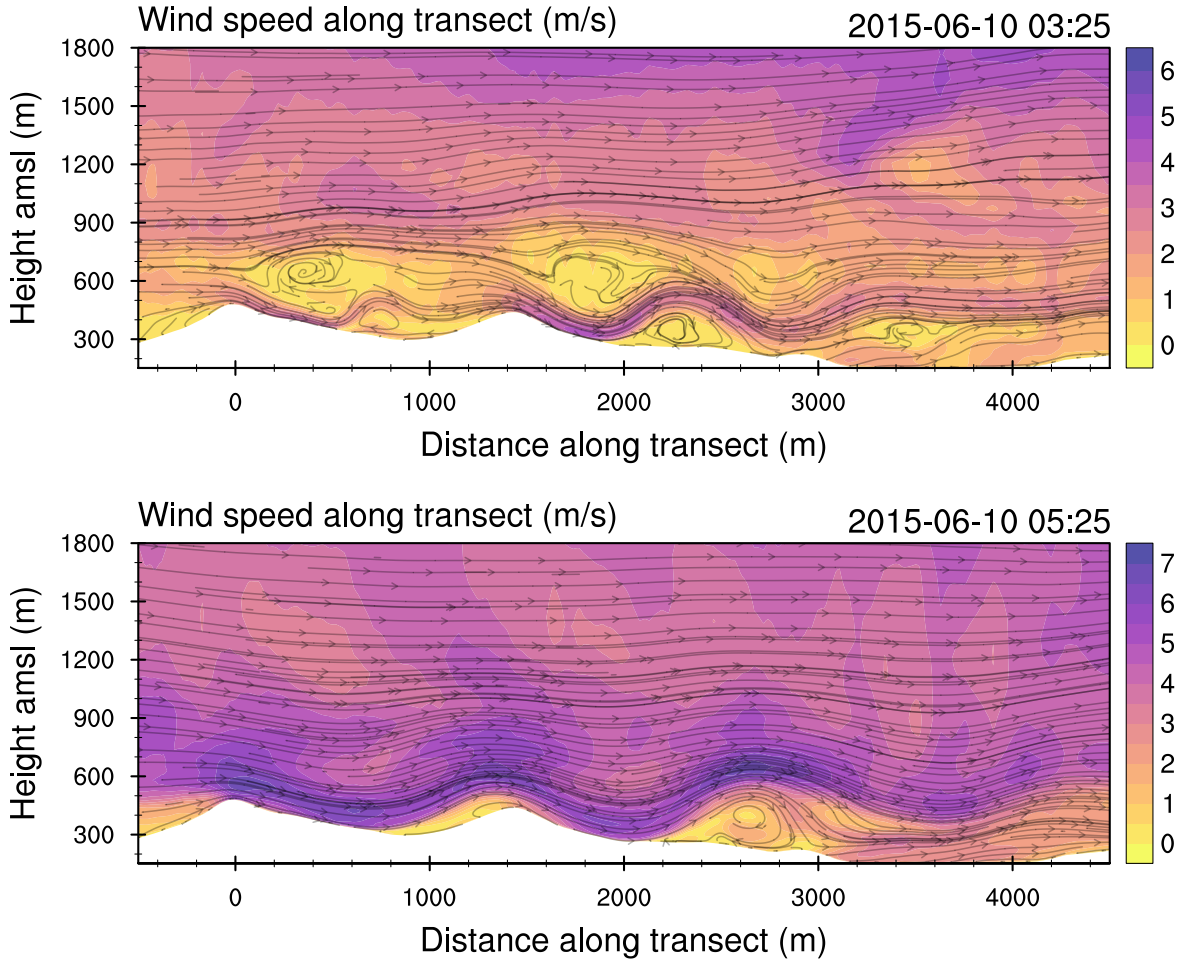

Figure 8: Simulation results for June 10$^{\text{th}}$ 2015 showing two different gravity waves regimes. The contour map shows the horizontal wind speed magnitude together with the flow streamlines.

In both cases the wave activity stops 3 km past the first ridge, which may happen as energy is dissipated due to friction. This kind of lee waves are associated to a decrease of the Scorer parameter with height [15]. Numerical experiments in the literature assuming inviscid flow usually resort to a sudden change in static stability to force wave resonance. In the present case the Scorer parameter did decrease with height, however this was due to the boundary layer near the surface instead of an inversion layer, as static stability varied smoothly with height.

4. Conclusions

Results from field experiments and numerical simulations of real wind conditions over a double-ridge topography were compared for a period of one day. The measurements were attained with the long-range WindScanner system. The simulations were performed by dynamical coupling using the WRF and VENTOS®/M atmospheric flow solvers, driven by ERA-Interim reanalysis datasets. The main conclusions are:

1. Comparison of the time series at the top of the first ridge showed a good agreement during the diurnal period, both in the wind speed and direction.
2. The nighttime was characterized by north-eastern winds and wind speeds around $5\,\mathrm{m\,s^{-1}}$.

The simulations predicted very low wind speeds with disagreements in the wind direction higher than 90°.

3. Vertical transects of the nocturnal flow field showed two distinct layers: an upper one with positive radial velocity values and a lower one with negative values. The simulations failed to reproduce the sign change, which was attributed to the direction error observed in the time series.
4. The simulations show a highly three-dimensional flow which is not aligned with the transect plane. It was estimated that a wind direction shift higher than 35°would be sufficient to have negative radial velocity values.
5. Both measurements and simulations show horizontally-repeating mountain waves and a valley rotor. The simulations further predict the existence of a leeward rotor past the second ridge and wave breaking after both of the ridge tops.
6. Two lee wave regimes were found in the simulations, one where the flow wavelength is similar to that of the orography and other where the flow wavelength is reduced to half. While the valley rotor was only present in the second regime, the leeward rotor was present in both regimes.

Acknowledgments

The present work benefited from the financial support of *Fundação para a Ciência e Tecnologia* under ERANET research project *NEWA – New European Wind Atlas* (NEWA/0001/2014).

References

[1] Vasiljević N 2014 *A time-space synchronization of coherent Doppler scanning lidars for 3D measurements of wind fields* Ph.D. thesis DTU Wind Energy, Denmark
[2] Berg J, Vasiljević N, Kelly M, Lea G and Courtney M 2015 *J. Atmos. Oceanic Technol.* **32** 518–527
[3] Drechsel S, Mayr G J, Chong M and Chow F K 2010 *J. Atmos. Oceanic Technol.* **27** 1881–1892
[4] NEWA 2015 New European Wind Atlas. European Commission ERA-NET+ project URL `http://www.neweuropeanwindatlas.eu`
[5] EOL 2015 Perdigão field experiment. Earth Observing Laboratory, University Corporation for Atmospheric Research URL `http://www.eol.ucar.edu/field_projects/perdigo`
[6] Skamarock W C, Klemp J B, Dudhia J, Gill D O, Barker D M, Duda M G, Huang X Y, Wang W and Powers J G 2008 A Description of the Advanced Research WRF version 3 Technical Note NCAR/TN-475+STR National Center for Atmospheric Research Boulder, Colorado, USA 113 pp.
[7] Veiga Rodrigues C, Palma J M L M and Rodrigues A H 2016 *Boundary-Layer Meteorol.* **159** 407–437
[8] Mann J, Palma J M L M, Matos J C, Angelou N, Courtney M, Lea G and Vasiljevíc N 2016 Experimental investigation of flow over a double ridge with several Doppler lidar systems Pres. at 96th American Meteorol. Soc. Annual Meeting URL `http://ams.confex.com/ams/96Annual/webprogram/Paper284781.html`
[9] Hansen K S, Larsen G, Menke R, Vasiljevíc N, Angelou N, Feng J, Vignaroli A, Liu W, Xu C and Shen W 2016 Wind turbine wake measurement in complex terrain Pres. at TORQUE2016 The Science of Making Torque from Wind (submitted)
[10] Pauscher L, Vasiljevíc N, Callies D, Lea G, Mann J, Klaas T, Hieronimus J, Gottschall J, Schwesig A, Kuehn M and Courtney M 2016 An inter-comparison study of multi- and DBS-lidar measurements in complex terrain *Remote Sensing* (submitted)
[11] ECMWF 2009 Era-interim project URL `http://dx.doi.org/10.5065/D6CR5RD9`
[12] Pineda N, Jorba O, Jorge J and Baldasano J M 2004 *Int. J. Remote Sens.* **25** 129–143
[13] Jiménez P A and Dudhia J 2013 *J. Appl. Meteorol. Climatol.* **52** 1610–1617
[14] Veiga Rodrigues C and Palma J M L M 2014 *J. Phys.: Conf. Ser.* **524** 012115 10pp.
[15] Teixeira M A C 2014 *Front. Phys.* **2** 1–24